IMAGING

Enabling precision monitoring of psoriasis treatment by optoacoustic mesoscopy

Benedikt Hindelang[1,2,3], Teresa Nau[1,2,3], Ludwig Englert[2,3], Andrei Berezhnoi[2,3], Felix Lauffer[1], Ulf Darsow[1], Tilo Biedermann[1], Kilian Eyerich[1], Juan Aguirre[2,3]*, Vasilis Ntziachristos[2,3,4]*

Psoriasis is a widespread inflammatory skin disease affecting about 2% of the general population. Recently, treatments that specifically target key proinflammatory cytokines driving the disease have been developed to complement conventional therapies with unspecific antiproliferative or anti-inflammatory effects. Efficient monitoring of treatment efficacy in the context of precision medicine and the assessment of new therapeutics require accurate noninvasive readouts of disease progression. However, characterization of psoriasis treatment remains subjective based on visual and palpatory clinical assessment of features observed on the skin surface. We hypothesized that optoacoustic (photoacoustic) mesoscopy could offer label-free assessment of inflammation biomarkers, extracted from three-dimensional (3D) high-resolution images of the human skin, not attainable by other noninvasive methods. We developed a second-generation ultra-broadband optoacoustic mesoscopy system, featuring sub–10-μm resolution and advanced motion correction technology, and performed 80 longitudinal measurements of 20 psoriatic skin plaques in humans under conventional inpatient treatment or receiving biologics with concomitant topical corticosteroid treatment. Optoacoustic image analysis revealed inflammatory and morphological skin features that indicated treatment efficacy with sensitivity, accuracy, and precision that was not possible using clinical metrics. We identify 3D imaging biomarkers that reveal responses to treatment and offer the potential to facilitate disease and treatment characterization. Our findings suggest that optoacoustic mesoscopy may offer a method of choice for yielding both qualitative and quantitative evaluations of skin treatments that are inaccessible by other methods, potentially enabling optimized therapies and precision medicine in dermatology.

INTRODUCTION

Affecting about 2% of the general population in Europe and North America, psoriasis is a widespread chronic inflammatory skin disease that severely impairs the quality of life and financially burdens the health care system and society (*1*). The disease is associated with a dysregulation of dendritic cells that produce, among other mediators, tumor necrosis factor–α (TNFα) and interleukin-23 (IL-23). In particular, the activation of T helper 17 (T_H17) cells, which release IL-17, contributes to the inflammation and metabolic activation of the skin. This includes the release of proangiogenic vascular endothelial growth factor. Phenotypically, histology of psoriatic skin exhibits hyperkeratosis, acanthosis, inflammatory cellular infiltrate, and a characteristic modified microvascular architecture. Macroscopically, the skin lesions present as demarcated erythematous plaques with adherent white scales (*1*, *2*).

There is no known cure for psoriasis. There is, however, strong interest in developing new treatments for managing the disease and suppressing the symptoms, and several treatment alternatives exist. Treatment is often required for a lifetime, but responses to therapies differ for each patient. Mild cases of psoriasis can be controlled by topical treatments using symptomatic descaling with agents like salicylic acid and broadly antiproliferative and anti-inflammatory drugs, such as corticosteroids, dithranol, and vitamin D derivatives, which modulate the local immune response and keratinocyte proliferation. Non- or mild responders to topical treatment may additionally require the administration of phototherapy or systemic drugs. Narrowband ultraviolet B (NB-UVB) phototherapy and psoralen-UVA (PUVA) photochemotherapy modulate inflammation by suppressing, among other effects, the T_H17 inflammatory pathway (*3*). Although topical treatment and phototherapy are effective in most cases, they are time-consuming and cannot be administered indefinitely. Conventional systemic therapies include methotrexate, acitretin, ciclosporin A, and fumaric acid esters, which nonspecifically target proinflammatory and proliferative pathways and are efficient in up to 50% of patients (*2*). Patients suffering from moderate to severe psoriasis who are treated with conventional therapies may experience recurrent relapses, repeatedly requiring expensive inpatient care. The introduction and ongoing development of biologics in recent years, mostly monoclonal antibodies targeting proinflammatory cytokines, such as TNFα (infliximab), IL-17 (Iexkizumab, brodalumab, and secukinumab), or IL-23 (ustekinumab and guselkumab), has revolutionized the treatment of patients for whom conventional approaches have failed, were contraindicated, or were not tolerated. Biologics are very effective with, for example, IL-17 inhibitors reducing disease severity by as much as 90% in about 70% of patients (*2*, *4*). Biologics are also safe and do not exhibit relevant cumulative toxicity or drug-drug interactions. However, biologics treatments are about 10 times more expensive than conventional treatments (about 15,000 to 25,000 €/year), which has largely restricted their role to second-line therapies (*2*).

Research into novel therapeutics and optimization of treatment requires accurate, precise, and longitudinal assessment of disease severity on an individualized basis. Ineffective therapies must be recognized, adapted, or changed as early as possible to avoid further

[1]Department of Dermatology and Allergy, Technical University of Munich, 81675 Munich, Germany. [2]Chair of Biological Imaging, Technical University of Munich, 81675 Munich, Germany. [3]Institute of Biological and Medical Imaging, Helmholtz Zentrum Munich, 85764, Neuherberg, Germany. [4]Munich Institute of Robotics and Machine Intelligence (MIRMI), Technical University of Munich, 81675 Munich, Germany.
*Corresponding author. Email: bioimaging.translatum@tum.de (V.N.); juanaguir@gmail.com (J.A.)

disease progression and excessive treatment costs. Adapting, for example, the frequency of biologics administration to the patient's response could make these therapies more cost-efficient. To fulfill the promise of personalized medicine, such evaluations require objective and quantitative grading methods. Given the strong interest in developing new psoriasis drugs, especially biologics, such grading methods are urgently needed to assess the efficacy of new therapeutics. In particular, a noninvasive method for assessing psoriasis would be highly desirable since the current gold standard of histology is inappropriate for longitudinal measurements. Disease severity is usually graded and monitored over time using clinical scores such as the psoriasis severity index (PASI), which is calculated from the percentage of affected body surface, redness (erythema), thickness (induration), and scaling of the psoriatic plaque as graded by visual and palpation assessment. The local PASI (or plaque PASI) is an alternative index that does not take into account the percentage of affected body and is used to monitor changes in psoriasis severity at a single location, e.g., at a single psoriatic plaque (*5*).

Despite the acceptance of the PASI or local PASI as disease severity metrics, palpatory and visual inspection is inherently subjective, offers only a surface view of the skin condition, has low sensitivity to capturing subtle changes in mild disease, and cannot assess or quantify critical pathological features within the skin (*6*). As an alternative, we consider herein ultra-broadband raster-scan optoacoustic mesoscopy (UB-RSOM) to resolve detailed three-dimensional (3D) images of psoriatic skin under treatment and investigate how skin microvasculature and other skin features relate to treatment response. Microvascular changes are increasingly being identified as important pathophysiological hallmarks of the underlying inflammation driving psoriasis progression (*7*, *8*) but cannot be accurately captured by PASI. Label-free imaging using UB-RSOM has recently afforded unique and highly detailed 3D images of the skin, resolving fine microvasculature and other skin morphological features that also serve as skin inflammation biomarkers (*9*–*14*).

To perform UB-RSOM, the region to be imaged is illuminated with low-energy short light pulses (~1 to 10 ns). The light travels through tissue, and a fraction of it is absorbed by chromophores, which, in turn, generate a tiny elevation of the local temperature (~0.001°C). As a result, ultrasound waves (photoacoustic/optoacoustic waves) are produced. The ultrasound waves are detected by an ultra-broadband transducer and processed mathematically using tomographic principles to obtain the 3D distribution of light absorbers (more information on the arrangement of the illumination and transducer below). This light-in–sound-out scheme enables the detection of optical absorption at acoustic resolution in deep tissue, as image formation is governed by the diffraction of generated ultrasound waves and not by the diffusion of light, overcoming the low penetration depth of classical optical microscopy techniques (~0.2 mm). Thus, UB-RSOM, when using visible or near-infrared light, produces 3D images of the most efficient light absorbers (hemoglobin and melanin) to resolve different skin features with up to sub–10-μm resolution, including capillary loops, the epidermis, and, critically, dermal vasculature over several millimeters of depth. The method is well suited for longitudinal observations of human skin because it is noninvasive and does not require the use of contrast agents. UB-RSOM yields superior 3D and cross-sectional visualizations of microvasculature compared to other optical imaging methods, such as confocal microscopy, multiphoton microscopy (MM) (*15*–*17*), optical coherence tomography (OCT), or high-frequency ultrasonography (*9*). With a detection bandwidth of more than 100 MHz, UB-RSOM offers the best combination of resolution and depth in dermatological imaging today (*18*) and enables previously inaccesible means and contrast mechanism to investigate skin parameters, disease, and response to treatment.

To accurately identify skin features that are most responsive to treatment, we developed a second-generation UB-RSOM (UB-RSOM 2G) system that overcomes past technological limitations by integrating advanced motion correction and a previously unknown skin placement design for repeatable data acquisition. We obtained 80 longitudinal UB-RSOM 2G scans from 20 psoriatic plaques under conventional treatment or receiving biologics treatment combined with topical corticosteroids (TCS) and reconstructed 3D skin images at 532 nm. Then, we used image analytics to understand how treatment acts on different inflammation-associated microvasculature features and which of these features are most sensitive to disease remission. A second goal of the study was to explore imaging biomarkers that could capture healing patterns that are not apparent to the human eye or the PASI, better accommodating the demands of personalized precision medicine. We observe three, previously unknown, microvascular features that exhibit high sensitivity to treatment and could improve the precision by which skin and inflammatory changes are assessed.

RESULTS

UB-RSOM 2G device and its ability to image psoriatic skin

The UB-RSOM 2G device (Fig. 1, A to C) consists of a scan head device that integrates a two fiber bundles illumination unit and a broadband focused ultrasound detector mounted onto a set of mechanical stages (Fig. 1C) with three degrees of freedom (x,y,z). The x and y axes are used to raster scan the ultrasound detector and optical fiber bundle over the imaged skin region. For each point of the raster scan, a light pulse illuminates the tissue, and the resulting optoacoustic wavefront is detected. The detected signals are filtered into two frequency bands for reconstruction: 10 to 42 and 42 to 120 MHz. A low-frequency band image (rendered in red) and a high-frequency band image (rendered in green) are correspondingly reconstructed, frequency equalized [see Materials and Methods and (*9*)], and coregistered. Multicolor rendering and frequency equalization allow for the observation of fine spatial details together with lower-resolution skin structures that generally have greater intensities. The smallest capillaries appear in green and can be resolved from the melanin structures that appear in red. The larger microvessels in the horizontal plexus appear in yellow and red and can be easily distinguished from the green capillary loops [see Fig. 1 and (*9*)].

The z axis allows the adjustment of the focal point of the transducer with respect to the skin surface. A control unit (Fig. 1B) integrates the laser source, alignment optics, data acquisition unit, and electronics. Repeated measurements of identical sections of the dermal microvasculature over the course of treatment were enabled by the combination of UB-RSOM 2G's detachable interface unit and the use of ink fiducial markers (see fig. S1) and the three degrees of freedom of the mechanical stages.

Application of UB-RSOM 2G to healthy and psoriatic skin (Fig. 1, D to G) allowed a side-by-side comparison of its performance in resolving relevant dermal features and confirms that UB-RSOM 2G produces detailed coronal (Fig. 1, D and E) and cross-sectional

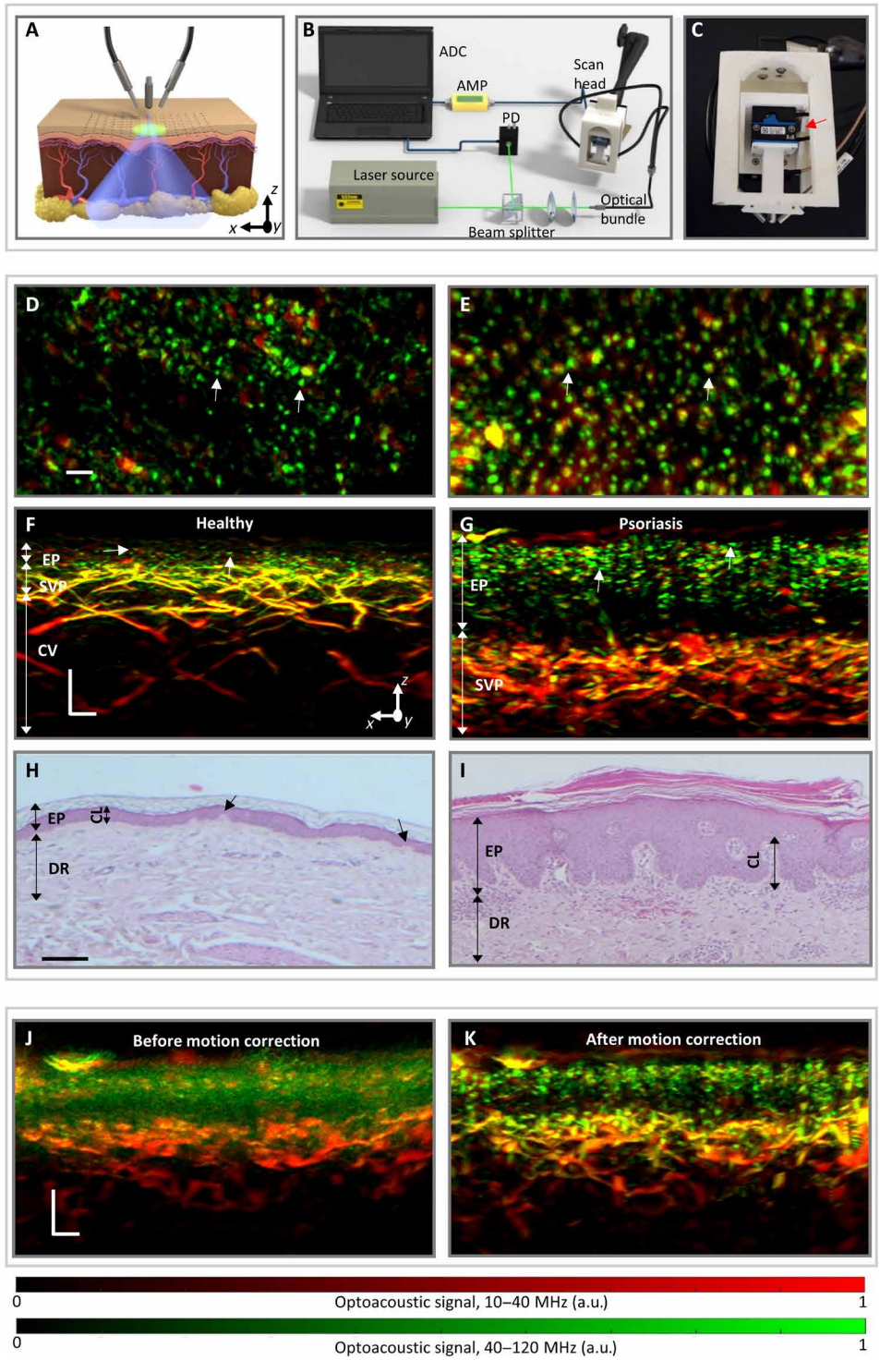

Fig. 1. Precision imaging of psoriasis using UB-RSOM 2G. (**A**) UB-RSOM 2G in use showing optical fiber bundles for illumination and a transducer that is raster-scanned parallel to the skin surface. (**B**) UB-RSOM 2G system. A laser pulse is directed to the sample. A part is diverged to a photodiode (PD), triggering the analog-to-digital convertor (ADC). The optoacoustic signals are amplified (AMP) and sent to the ADC. The transducer is in the scanning head. An interface unit ensures proper attachment to the skin. (**C**) Photograph of the scanning head with three stages, each of them a spatial axis (red arrow). (**D**) UB-RSOM 2G coronal section of healthy epidermis (EP) and dermal rete ridges containing capillary loops (CL; green dots, white arrows). (**E**) UB-RSOM 2G coronal section of the epidermis and dermal rete ridges of psoriatic skin. (**F**) UB-RSOM 2G cross-sectional image of healthy human skin showing the EP and vessels in the dermis consisting of the subepidermal vascular plexus (SVP) and the connecting vessels (CV). CL tips are visible (white arrows). Double-headed arrows indicate the layers containing the EP, SVP, and CV. (**G**) UB-RSOM 2G cross-sectional image of psoriatic skin. CL (white arrows) appear in green, interleaved with widened epidermal structures (EP, red). A dilated and dense widened SVP is also present. Double-headed arrows indicate the layers containing the EP and SVP. (**H**) Histological cross section of the same area depicted in (D) and (F). Small rete ridges can be observed, which contain the CL (black arrows). (**I**) Histological cross section of the same area as depicted in (E) and (G) showing acanthosis, hyperkeratosis, and elongated CL. The SVP in the upper dermis (DR) appears dilated. (**J** and **K**) UB-RSOM 2G image of psoriasis before and after motion correction. Scale bars, 200 μm. a.u., arbitrary units.

images (Fig. 1, F and G) of the skin. These images reveal the epidermis and the underlying dermal structures. In healthy skin, the melanin in the epidermis and the capillary loops in the dermal rete ridges, which are interwoven with the epidermis, are clearly resolved. In the deeper dermal layer, the subepidermal vascular plexus and connecting vessels are visible. This general appearance changes in psoriatic skin, wherein UB-RSOM 2G captures the underlying acanthosis, the drastic elongation and dilation of the capillary loops, and an expansion of the subepidermal vascular plexus.

Histological analysis of regions scanned by UB-RSOM 2G corroborate the in vivo findings (Fig. 1, H and I). The histological slice of the healthy skin section (Fig. 1H) corresponding to the UB-RSOM 2G image in Fig. 1 (D and F) shows the different layers of the epidermis and an ordered maturation of the keratinocytes. The thickness of the epidermis (123 μm) as measured from the subepidermal plexus to the skin surface by UB-RSOM 2G agrees with that observed in the histological slice (115 μm). The lengths of the capillary loops extending through the rete ridges are typical of healthy skin (Fig. 2F, white arrows) (*9*). Observation of the histological cross section of the psoriatic plaque (Fig. 1I) corresponding to the

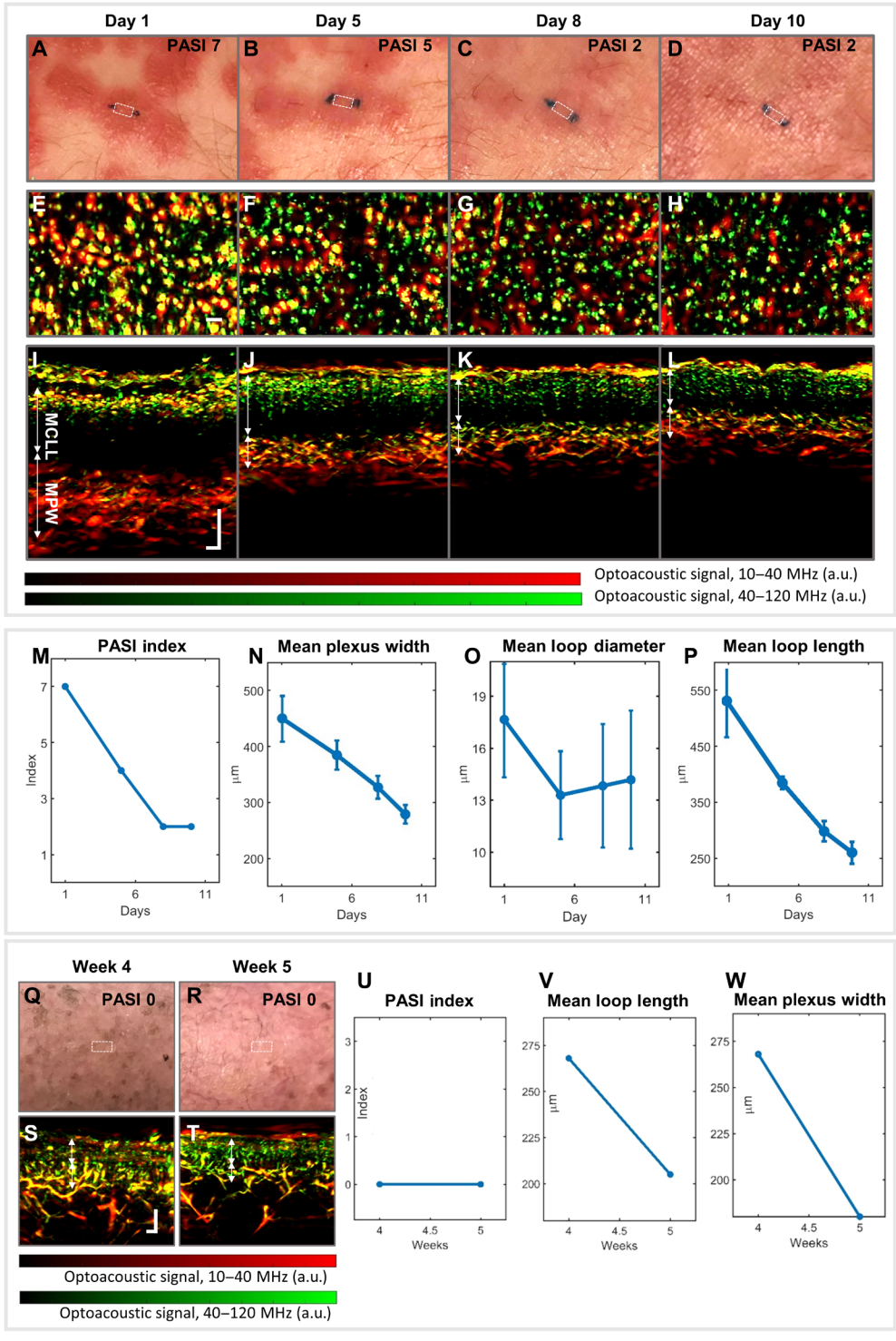

Fig. 2. Clinical views of psoriatic plaque during conventional therapy and the corresponding coronal and cross-sectional UB-RSOM 2G images. (**A** to **D**) Clinical photographs of the same psoriatic plaque on days 1, 5, 8, and 10 of conventional treatment with the PASI value indicated in the top right. Ink fiducial markers (two dark green dots) ensure that the imaged section of the dermal vasculature is reproduced (see fig. S1). (**E** to **H**) Coronal UB-RSOM 2G images corresponding to the white dotted rectangles in the clinical photographs in (A) to (D). The images are at the depth of the epidermal layer. Dots correspond to CL. Color shift from red or yellow to green indicates an increasing proportion of high-frequency content within the ultrasound signal emanating from smaller microvessels. (**I** to **L**) Cross-sectional UB-RSOM 2G images corresponding to the white dotted rectangles in the clinical photographs in (A) to (D). The tips of the CL appear as dots, whereas the perpendicular sections of the loops cannot be imaged and appear as black areas. Mean capillary loop length, MCLL; mean plexus width (mean width of the SVP), MPW. Scale bars, 250 μm. (**M**) Local PASI during treatment. (**N**) MPW. (**O**) Mean capillary loop diameter (MCLD) and (**P**) MCLL. (**Q** and **R**) Clinical imaging of psoriatic skin of a patient undergoing biologics treatment. Visual inspection on weeks 4 and 5 of treatment revealed no pathology, and consequently, the PASI index value was graded zero. (**S** and **T**) UB-RSOM 2G imaging of affected skin (white dashed rectangles) in (Q) and (R). (**U** to **W**) Local PASI index, MCLL, and MPW of skin in (Q) and (R). Scale bars, 200 μm.

UB-RSOM 2G image in Fig. 1 (E and G) shows hyperplastic epidermis pathology with aberrant replication of keratinocytes and the elongation of the rete ridges. The elongated capillary loops "climb" through the rete ridges, a feature that is captured in vivo by UB-RSOM 2G (Fig. 1G, white arrows). UB-RSOM 2G uses advanced motion correction algorithms to compensate for slight involuntary movements of the patients' body (Fig. 1, J and K, and Materials and Methods), which proved to be effective for psoriatic skin.

To assess in detail the ability of UB-RSOM 2G to quantify treatment efficacy, we longitudinally monitored 14 identical sections of 14 psoriatic plaques from 14 patients undergoing conventional inpatient treatment over the course of several days and six psoriatic plaques from five patients during the initial phases of out-patient biological treatments over the course of several weeks. Conventional inpatient treatment included daily application of standard topical doses of salicylate vaseline, corticosteroids, dithranol, and simultaneous phototherapy (311-nm NB-UVB or PUVA). Patients in the biologics group, in addition to continuing their previously ineffective standard TCS therapy, received the IL-17 inhibitor secukinumab (four patients, subcutaneous injection) or the TNFα inhibitor

infliximab (one patient, intravenous injection) according to the respective initiation scheme. For every patient, we analyzed coronal images of the epidermis and cross-sectional images corresponding to the whole skin depth. The latter provided a comprehensive view of the microvascular structure, whereas the former depicted the appearance of the capillary loops (Fig. 1, D to G).

UB-RSOM 2G biomarkers of psoriasis

A critical point herein was to examine the effect of treatment on different microvascular and other skin features that are uniquely resolved by UB-RSOM. We were interested to study whether different features respond differently to treatment, and which features were most sensitive to treatment and disease remission. The changing appearance of a representative plaque during the course of conventional treatment is displayed in Fig. 2. We obtained clinical and UB-RSOM 2G images before (day 1) and on days 5, 8, and 10 of the treatment (Fig. 2, A to L). We imaged the same location on the psoriatic plaque at every time point by making use of ink fiducial markers (see fig. S1). The clinical images (Fig. 2, A to D) show how the plaque improved from an initial severity visual score of PASI = 7 to a score of PASI = 2 at days 8 and 10 due to a major reduction in redness and induration. The corresponding UB-RSOM 2G coronal views of the epidermis views show that the diameters of the capillary loops clearly decrease from the initial measurement to day 5, after which they appear to stabilize (Fig. 2, E to H). The UB-RSOM 2G cross-sectional perspectives (Fig. 2, I to L) of the whole dermal depth reveal a more complete picture of how the treatment affects the microvascular structure of the psoriatic skin. Initially, the microvessels in the plexus appear densely packed and are barely resolved due to vasodilation and angiogenesis associated with the underlying inflammatory process (Fig. 2I). As a result, the subepidermal plexus appears both thick [as indicated by the mean plexus width (MPW) in Fig. 2I] and dense. As treatment progresses, the microvascular stress supporting the inflammatory milieu decreases, with a subsequent reduction in the mean width of the subepidermal plexus (Fig. 2, J to L). Moreover, by day 8, the individual microvessels can be discerned due to a reduction in tortuosity and vasodilation (Fig. 2K). The cross-sectional images also reveal how the lengths of the capillary loops decrease drastically.

This qualitative assessment of UB-RSOM 2G features was corroborated by image analysis to quantitatively study the relevance of particular skin features in relation to treatment progression. We extracted the mean capillary loop length (MCLL), mean capillary loop diameter (MCLD), and mean width (thickness) of the subepidermal vascular plexus (MPW) because they correlated with the clinical response to treatment (improvement from PASI = 7 on day 1 to PASI = 2 on day 8; Fig. 2M). These three metrics relate directly to microvasculature, which is prominently affected by inflammation (*19*). The MPW decreased during the days of observation, from 0.46 to 0.29 mm (Fig. 2N). The MCLD, which corresponds to the mean width of the individual capillary loops measured in top view, decreased during the first 5 days of treatment, from an initial value of ~18 μm to stabilize between 13.5 and 14 μm (Fig. 2O). The MCLL exhibited consistent improvement with therapy over time, which manifested as an overall reduction in length from 0.55 to 0.27 mm (Fig. 2P), approaching the "healthy length" [~0.08 mm; (*20*)].

In several cases, RSOM data recorded therapeutic effects over time that were not captured by the PASI. For example, one case demonstrated no change in PASI between days 8 and 10 (Fig. 2, A to L), whereas the MPW and MCLL showed clear evidence of skin recovery during the same time period (Fig. 2, N to P). We also observed cases where the PASI indicated that psoriatic skin was healed (Fig. 2, Q and R), whereas UB-RSOM 2G revealed residual pathological features of psoriasis (Fig. 2, S and T). These data were taken from a patient receiving biologics treatment. Despite the PASI indicating that complete healing was achieved at week 4 (Fig. 2U), UB-RSOM 2G imaging revealed a persisting but recovering pathological architecture of the microvasculature from weeks 4 to 5. In particular, UB-RSOM 2G recorded an MCLL decrease of 24% (from 264 to 200 μm) and an MPW decrease of 19% (from 367 to 298 μm; Fig. 2, V and W).

UB-RSOM 2G ability to monitor treatment

Observations of individual patients demonstrate the ability of UB-RSOM 2G to reveal highly detailed images of treatment and quantitatively compute image metrics that showcase higher sensitivity than PASI; however, we also studied the ensemble of data to understand the trends in the entire collected dataset (Fig. 3). We plotted UB-RSOM 2G features, serving as treatment biomarkers, for all patients treated with conventional in-patient treatment (Fig. 3A and fig. S2A) or with biologics (Fig. 3B and fig. S2A) and extracted mean trends. The results were again contrasted with the current gold standard PASI both qualitatively and by calculating correlation values. Before treatment, the local PASI was similar in both groups, with a mean of 5.6 (range, 4 to 8) in the conventional treatment group and a mean of 5.0 (range, 3 to 9) in the biologics treatment group (fig. S2A). After 6 to 13 weeks, the plaques treated with biologics healed better (mean PASI 0.6; three of six reached PASI 0) than the plaques undergoing conventional treatment over the course of 9 to 10 days (mean PASI 2.2; 1 of 14 reached PASI 0). The MCLL decreased monotonically in all patients (Fig. 3, A and B). During conventional treatment, the MCLL decreased, on average, from a value of 399 to 253 μm (−36.6%). The MPW also decreased monotonically for most patients and time points, declining by an average of 26.0% over the course of conventional treatment (Fig. 3A). Analogous trends in the MCLL and MPW were observed for the patients treated with biologics (Fig. 3B). The MCLD decreased with treatment in all skin sections, but its reduction was not as consistent as that of MCLL and MPW. The MCLL showed a great degree of correlation with PASI for both types of treatments (0.78, $P = 2 \times 10^{-5}$ for biologics and 0.74, $P = 2 \times 10^{-10}$ for conventional). The MPW showed a lower correlation with the PASI (0.52, $P = 0.01$ for biologics and 0.60, $P = 2 \times 10^{-6}$ for conventional), whereas the MCLP displayed the lowest correlation (0.48, $P = 0.03$ for biologics and 0.53, $P = 2 \times 10^{-4}$ for conventional (Fig. 3, C to E).

To offer an objective index that describes psoriasis remission and inflammatory burden, we compiled the quantified biomarkers into a psoriasis optoacoustic severity index (POSI; fig. S2B). The POSI combines the severity metrics of the MPW and the MCLL, i.e., the two biomarkers that were unambiguously affected by treatment. POSI mimics the local PASI, which could facilitate its clinical acceptance. More specifically, POSI showed good correlation with the local PASI in this study ($r^2 = 0.77$, $P = 0.00004$; fig. S2C) while also capturing subtle changes not reflected in the PASI scores.

In a pilot observational study, we compared the findings between patients treated with conventional therapy and patients treated with biologics. In particular, we compared the percentage change of the PASI with that of the UB-RSOM 2G biomarkers (fig. S3) in both

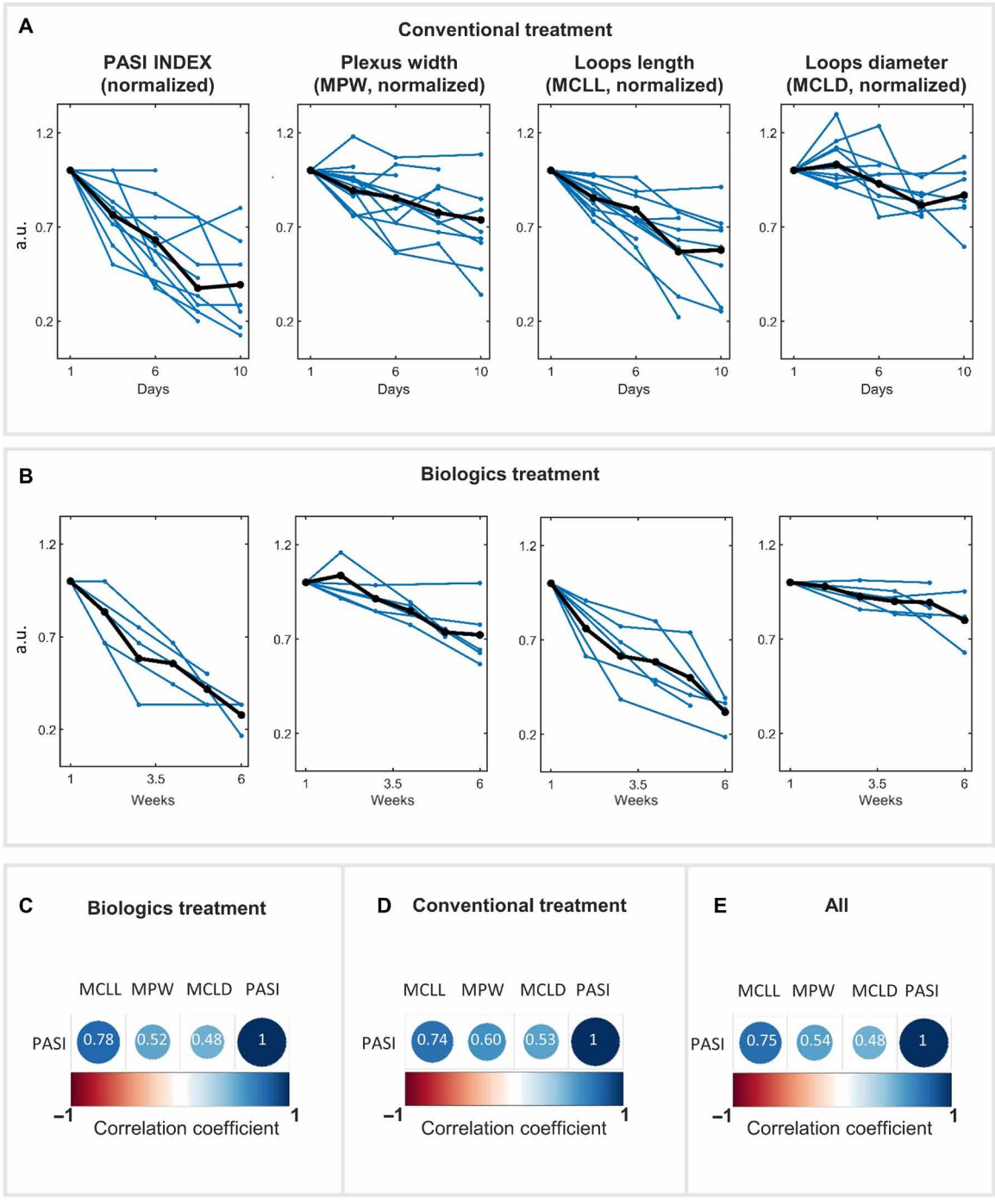

Fig. 3. Change in UB-RSOM 2G biomarkers during psoriasis treatment. (**A**) The evolution of each of the RSOM features (biomarkers) over time for patients receiving conventional treatment. Blue lines represent each individual patient, and black lines represent the average. (**B**) Each graph shows the evolution of each RSOM biomarkers as a function of the biologics treatment time. (**C**) Correlation coefficients between PASI and the RSOM biomarkers calculated for the patients undergoing biologics treatment. (**D**) Correlation coefficients between PASI and the RSOM biomarkers calculated for the patients undergoing conventional treatment. (**E**) Correlation coefficients between PASI and the RSOM biomarkers calculated for all patients.

patient groups. For patients undergoing conventional treatment, the MCLL, MPW, and MCLD decreased at similar rates during the initial phase of the treatment, whereas in patients treated with biologics, there was a steeper decrease in the MCLL. This could indicate that during biologics treatment, the length of the capillary loops and possibly the strongly associated palpable and visible plaque induration decrease faster, while other pathological features of the microvascular architecture that are invisible to superficial clinical assessment may persist. An observation of this effect has not been possible until now. Although the clinical implications remain

unclear, and the analysis was based only on a small number of patients, this result demonstrates the potential of UB-RSOM 2G to yield deeper insights into the physiology of both the disease and its treatment.

Repeatability study

The variable pressure exerted by the scan head on the skin might compress the dermis and corrupt biomarker calculations. To confirm the quality of the data and that the fine differences captured by RSOM 2G were not the result of noise, motion, or errors introduced by the device operator during data collection, we conducted a repeatability study. Data were acquired from nine plaques at two time points, 10 min apart, after removing and repositioning the RSOM scan head between scans, guided by the ink fiducial markers. UB-RSOM 2G biomarkers were computed for all images, and a repeatability coefficient was calculated using an analysis of variance (ANOVA) model (*21*), which represents the absolute difference between two repeated results with a probability of 95%. The differences in the t = 0 min and t = 10 min time points revealed that repeating the scan head placement affords only small discrepancies in positioning of a few hundred micrometers (Fig. 4, A and B). As a result, in some cases, we observed that the images captured at the two time points were shifted relative to each other; however, matching anatomical features could be easily recognized in both images. The computation of UB-RSOM 2G biomarkers showed little difference in values between t = 0 and t = 10 min. For example, the MCLL and MPW values showed a repeatability coefficient of 36.7 and 38.4 μm, respectively (Fig. 4, C to E).

For the three computed biomarkers (MCLL, MPW, and MCLD), the quantification accuracy is given by the axial resolution of the system. The RSOM system used here has a resolution of ~7 μm through the whole dermis (*9*), which implies that both repeatability analysis and the overall trends observed in Figs. 2 and 3 are not affected by the system's resolution. The repeatability study also showed that the biomarker changes computed as a function of treatment were not a result of system or operator errors (e.g., the effect of variable pressure on skin) but instead represent true microvasculature changes due to the treatment and disease remission. For example, in the case corresponding to the difference between days 8 and 10 shown in Fig. 2, the MPW decreased by 56 μm and the MCLL decreased by 49 μm, whereas PASI remained constant (Fig. 2, M, O, and P) and the repeatability coefficients are 38.4 and 36.7, respectively.

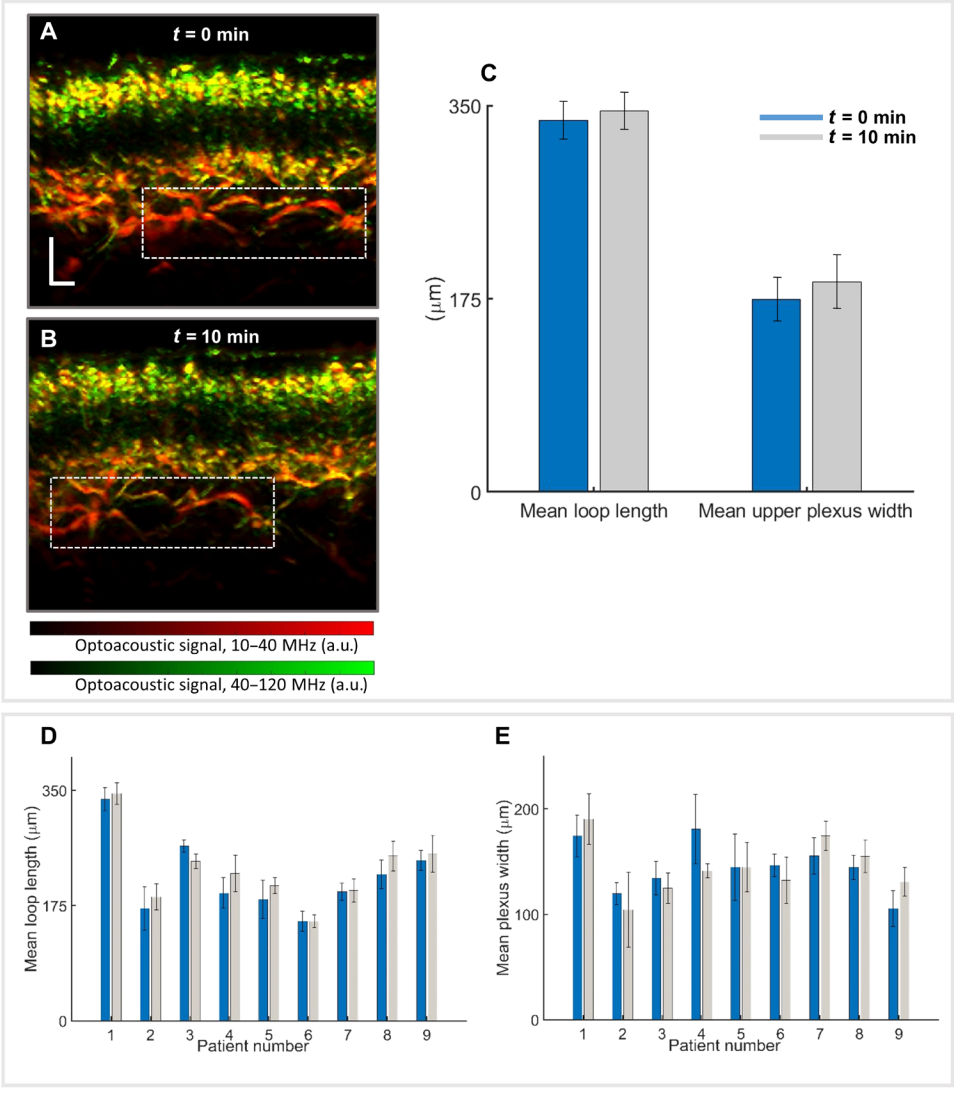

Fig. 4. Repeatability of biomarkers extracted from UB-RSOM 2G measurements. (**A** and **B**) Sample images for one patient from the repeatability study. An initial image was recorded (t = 0) followed by a second image after 10 min (t = 10). The dashed rectangle shows the same structure in both images. It can be observed that the scan head could not be placed at the identical position in both measurements. The positioning error was about 900 μm. (**C**) Values of the MCLL and MPW corresponding to images (A) and (B). The measurement could be repeated within a difference of a few tens of micrometers. (**D**) Values of the MCLL calculated from both measurements (t = 0 and t = 10 min) for each patient. (**E**) Values of the MPW calculated from both measurements (t = 0 and t = 10 min) for each patient. Scale bars, 200 μm.

Correlation between the RSOM biomarkers and DLQI

Quantitative markers of treatment as afforded by the UB-RSOM 2G biomarkers are useful for assessing response to treatment; however, it is important to also consider more subjective indications of treatment efficacy, such as patient-reported symptoms. We therefore gathered response-to-treatment dermatology life quality index (DLQI) data for 83% of the biologic therapy patients (fig. S5). We found a positive correlation for both the MCLL (Pearson correlation

coefficient of 0.72, $P = 0.008$) and the MPW (Pearson correlation coefficient of 0.78, $P = 0.003$). DLQI was not available for the patients who received conventional therapy.

DISCUSSION

In this study, we monitored the treatment of psoriasis using computed biomarkers extracted from detailed 3D images including epidermis and dermis generated by a UB-RSOM 2G device with advanced placement and motion correction technology. This approach is markedly different from the current method of psoriasis assessment, which only evaluates response based on subjective visual and palpatory examinations of lesions by physicians. By providing a complete picture of the disease, including subsurface features at resolutions of 10 μm or better, UB-RSOM 2G affords more detailed observations of inflammatory features based on microvasculature and other morphological biomarkers. Furthermore, this study yielded unprecedented insights into the effects of conventional and biologics treatments on psoriatic lesions. We found that treatments led to large changes in the length of the capillary loops and the width of the subepidermal plexus. Such changes continue even when clinical evaluation (PASI) indicates that a plaque is unchanging. Elongation of the capillary loops is a well-known marker of psoriatic skin in histological assessment (*1*). However, until now, this parameter could not be directly and noninvasively quantified in vivo.

We found the MCLL and MPW to be the most sensitive parameters to treatment. These biomarkers could be used to construct the POSI, which could offer a more precise index than PASI for treatment and disease characterization. MCLL and MPW elucidated changes in skin microvasculature that were more subtle than those revealed by the more subjective PASI grading. The MCLL and MPW thus allowed us to observe and quantify improvements in psoriatic skin where no visible change was apparent or recorded by the PASI, which reflects the high accuracy and precision of RSOM. A quantitative comparison between the accuracy and precision of the RSOM biomarkers and the PASI components is not a straightforward task because of the subjective nature of the latter. However, some conclusions can be derived. For example, it is generally accepted that the accuracy of the induration component of the PASI (thickness of the plaque) is 250 μm, which corresponds to the resolution of the average human eye. This implies that the RSOM biomarkers improve upon the accuracy of the PASI component by two orders of magnitude (the axial resolution of UB-RSOM 2G is ~7 μm). On the other hand, the concepts of "redness" and "degree of scaling" included in the PASI are difficult to put into context against the micrometer resolution biomarkers obtained by RSOM. Overall, the objective nature of optoacoustic biomarkers (precision) and their low error due to the method's high resolution (accuracy) lead to better sensitivity. Higher sensitivity here means that UB-RSOM 2G is able to show healing effects that were not previously detectable by clinical assessment and reveals subtle pathology when the PASI indicates healthy skin. For the sake of completeness, we have to point out that we also found that the measurements of MCLD were slightly affected by blurring due to unknown sources of error, which may include wrong reconstruction parameter estimation.

The ability to observe fine skin parameters associated with inflammatory burden could both improve and personalize treatment monitoring and drug development. The quantification of changes in representative portions of the skin during treatment with high sensitivity to therapy could lead to more accurate assessments of treatment efficiency, serving the goals of precision medicine by offering objective biomarkers that are urgently needed (*22*). UB-RSOM 2G could aid in selecting the most suitable therapy for an individual and in the precise monitoring of the patient's early response to treatment. Considering the high long-term costs of psoriasis therapy, particularly when using biologics, individualized therapies (e.g., tailored application frequencies) would benefit both the patient and the health care system. New metrics are also needed for drug development, because PASI lacks responsiveness and sensitivity in the case of mild disease (*6*). New biologics for psoriasis treatment are being developed and continue to enter the market. Because of their overall high efficacies, it is increasingly important to be able to observe slight differences in treatment response not allowed by PASI. UB-RSOM 2G could therefore be useful for drug discovery or clinical decision-making about treatment selection and drug dosing. By revealing pathological states of skin not detectable by the current standard, the use of optoacoustic biomarkers could improve decisions regarding treatment termination and areas of application, the latter for the specific case of topical conventional treatment.

UB-RSOM 2G offers compelling advantages for treatment assessment over other imaging methods in dermatology. Optical microscopy methods, such as reflectance confocal microscopy (RCM) and MM, can image superficial pathological features of psoriatic skin, such as parakeratosis, spongiosis, inflammatory cells, and the dilation of the capillary loops. However, the typical penetration depths of ~100 μm for RCM and MM are insufficient to visualize the subepidermal vascular plexus or precisely measure the full lengths of microvessels from their origins in the plexus. Even psoriatic plaques with "moderate" induration according to PASI grading can reach thicknesses of 0.5 mm or more. OCT and high-frequency ultrasound (HFUS) can offer deeper imaging. Pilot OCT studies found that the epidermal thickness may decrease during psoriasis therapy, but although the changes were statistically significant, they were small in magnitude and do not allow for a direct assessment of the underlying inflammation (*23*–*28*). Although OCT-based angiography can visualize superficial microvessels, the method is inappropriate to comprehensively assess the capillary loops and image the subepidermal vascular plexus in thickened psoriatic skin, since it cannot produce high-quality 3D images of the skin due to strong inherent artifacts in the axial direction (*29*–*31*). Moreover, the optoacoustic contrast from microvessels, which stems from the strong optical absorption of hemoglobin, is superior to that of OCT, which indirectly detects blood via flow-related signals. The contrast of microvessels is even poorer in HFUS. Label-free HFUS only detects vessels larger than 100 μm (*32*), which is far above the diameter of most dermal microvessels. Photography-based machine learning algorithms have recently been introduced, which are capable of determining local PASI and the affected body surface (*33*). While these methods can be more objective and reliable than conventional PASI assessments, their dependence on superficial information fundamentally limits these methods to the same features evaluated by PASI. Integrating such methods with RSOM could eventually afford a most powerful approach for the determination of psoriasis severity.

With the recent evolution of laser-diode sources with the potential to reach sufficiently high-energy levels for RSOM (*34*), the UB-RSOM system is expected to have a cost of components in the

few thousands of euro range, with mass production further reducing this cost. At such cost of materials, the technology offers a viable solution for dermatology clinics and high dissemination potential. Nevertheless, several improvements to the UB-RSOM 2G system are being made based on feedback from clinical users to overcome practical constraints that may hinder the wide adoption of the technology. One such future development is the construction of an enclosed interface unit with automatic water filling to avoid leakage and enable imaging at tilt angles that are higher than the 30° angle that is currently possible. Another future development is directed toward adding an optical camera detector that can use pattern recognition methodology based on anatomical references to avoid the necessity of fiduciary for ensuring repeatable placement on the same skin location over longitudinal measurements. Such improvements can also reduce the procedure time that it takes to obtain a scan. Now, a trained user can place the system and obtain an image in 7 to 10 min. Next-generation systems will aim to be able to place the system on the skin and obtain the required image in about 1 min.

Clinical acceptance of a previously unknown modality is a complex process that depends on multiple parameters, including cost, overall benefit, ease of use, health risk, and overall performance related to the state of the art. UB-RSOM 2G is a strong candidate for future routine use in dermatology because it is a noninvasive optical technique with unique imaging capabilities. UB-RSOM 2G could provide objective precision measurements of subsurface skin features that augment scores of a patient's subjective symptoms and quality of life to improve clinical decision-making. Preliminarily, we showed that the response to therapy seen by the RSOM biomarkers correlated with the DLQI for a subset of patients; however, future studies should focus on correlating objective readings with subjective symptoms. Our results indicate that UB-RSOM 2G is well suited to observe and quantify treatment success in representative psoriasis plaques. Further work will elucidate if measuring a greater number of plaques in different parts of the body will prove more beneficial for quantifying the overall treatment success.

In this second-generation system, we have already incorporated methods for improved placement and motion correction to offer accurate measurements in a portable, handheld format. Further work should optimize the water handling and the acquisition time for a better compatibility of the system in the clinical routine. The repeatability study showcased that, although the resolution of the system is ~7 μm, the precision of the system was ~36 to 38 μm due to motion and placement errors. We anticipate that this pilot study will trigger a larger range of independent investigations into novel psoriasis pharmaceuticals. It is critical that such future studies quantify reproducibility in a manner similar to the present work to clearly identify the accuracy of the method at different operator experiences. It is important to compute the interoperator error to identify whether new designs for placement and motion correction are required to further improve the precision toward the theoretical limit (<10 μm).

MATERIALS AND METHODS

Study design

Response to treatment

The protocol for the therapy response study was approved by the Ethics Committee of the Faculty of Medicine of the Technical University of Munich. A total of 19 patients participated in the study (14 men and 5 women; age, 22 to 68 years; mean age, 44.1 years) after giving written informed consent. All participants were patients of the Department of Dermatology at the university hospital of the Technical University of Munich and had been diagnosed with plaque psoriasis, which was confirmed by histology. The study included one group (group A) of patients undergoing conventional and one group (group B) of patients being treated with biologics in addition to continuing their previously ineffective therapies with TCS. Fourteen patients were monitored during conventional inpatient treatment consisting of topical descaling, anti-inflammatory therapy (by means of salicylate vaseline, TCS, and dithranol), and simultaneous phototherapy (311-nm NB-UVB or PUVA). The first measurement was performed using the UB-RSOM 2G immediately before therapy, and measurements were taken on day 1 (14 plaques), day 3 (12 plaques), once between days 4 and 6 (9 plaques), once between days 7 and 8 (9 plaques), and once between days 9 and 10 (9 plaques). The fact that not all patients could be measured at all time points was due to limits on the durations of their stays in the hospital and lack of patient access on weekends. A procedure using ink fiducial markers was established to image the same section of the psoriasis plaques over time (fig. S1). The five patients included in group B were imaged before and during therapy with the biologics infliximab (one patient) and secukinumab (four patients) and standard TCS therapy. In one of these patients, two plaques were monitored, resulting in six plaques examined in group B. Measurements were taken before therapy at week 1 (six plaques), week 2 (two plaques), week 3 (three plaques), week 4 (three plaques), week 5 (four plaques), and once between weeks 6 and 13 (five plaques). By using photos and anatomical landmarks, the imaged part of the monitored psoriasis plaques was kept as similar as possible between the measurements. Histology was taken once from the monitored plaque in one patient before undergoing conventional treatment.

Repeatability

The therapy response study protocol was approved by the Ethics Committee of the Faculty of Medicine of Technical University of Munich. A total of nine patients participated in the study (four men and five women; age, 19 to 51 years; mean age, 32.1) after giving written informed consent. All participants were patients of the Department of Dermatology at the university hospital of the Technical University of Munich and had been diagnosed with plaque psoriasis, which had been confirmed by histology. The repeatability study was designed following the guidelines that can be found in (*21*). For each patient, two measurements of the same plaque were recorded 10 min apart using the UB-RSOM 2G. After the first measurement, the scan head was completely removed from the patient and replaced after 10 min. Between measurements, the patient was free to move or walk. The ink fiducial marker procedure was used for placements of the scan head. The MCLL, MPW, and MCLD parameters were derived for each measurement using the same procedure as described below for the conventional psoriasis therapy monitoring study.

UB-RSOM 2G system, motion correction, and image reconstruction

The UB-RSOM 2G system was built in-house. For light excitation, the system uses a 532-nm Nd:YaG laser (Wedge HB.532, Bright Solutions Srl) at a pulse length of 0.9 ns to induce the broadband optoacoustic signals. Experiments were conducted using a 500-Hz repetition rate, at which the light energy delivered to the skin surface does not exceed 3.75 μJ/mm^2, thereby complying with the

safety limits of laser exposure specified by the American National Standards Institute. The UB-RSOM 2G system scan head includes a spherically focused piezoelectric transducer (frequency range, 10 to 120 MHz) with a central frequency of 55 MHz (Sonaxis). The transducer is attached to three motorized stages: the *x*,*y* stages (size, 35 mm by 35 mm by 15 mm; Physik Instrumente) and the *z* stage (MTS50-Z8, Thorlabs). The *x*,*y* stages are used to scan the transducer and fiber bundles along a grid that yields a 4 × 2 mm field of view. The acquisition step is 20 μm, and the acquisition time is 70 s (8.75 s/mm^2).

The scan head also integrates the illumination bundles. An interchangeable interface unit shielded with an optically and acoustically transparent plastic membrane is placed below the scan head. The interface unit is filled with 1.5 ml of water and enables the acoustic coupling between the skin and the transducer detection surface. Once the unit is filled, the system is easily placed onto the desired skin area.

Before scanning, the *z*-axis motorized stage is used to place the transducer at the desired height above the skin surface (the focal point should be ~100 to 300 μm above the skin). After acquisition, the detected signals are filtered using a fourth-order butterworth filter into two frequency bands for reconstruction: 10 to 42 and 42 to 120 MHz. A low-frequency band image and a high-frequency band image are correspondingly reconstructed by applying the so-called universal back projection algorithm (*35*) to account for the out-of-focus signals. For representation, an RGB image is constructed in which the low-frequency band reconstruction occupies the red channel and the high-frequency reconstruction occupies the green channel. The high-frequency reconstruction is multiplied by a parameter, which is calculated by solving the optimization problem described in (*9*). Such an equalization operation increases the intensity of the high frequencies, partially taking into account the effects of the acoustic absorption in tissue, enabling size-dependent discrimination of tissue structures [see Materials and Methods and (*9*)] and their coregistration. Further technical details of the system have been described in (*9*). Major improvements in comparison to previous versions of UB-RSOM include the use of a motorized *z*-stage for precise adjustment of the ultrasound transducer's focal point slightly above the skin surface and the implementation of a motion correction algorithm (*36*) that improves the sensitivity of the reconstruction image to motion over previously published methods and was applied for psoriasis imaging for the first time. In such studies, the success of the motion correction algorithm relied on the presence of artifacts in the acquired data generated by the epidermal melanin layer. However, there is a notable reduction in melanin in psoriatic skin, reducing the effectiveness of the algorithm. The system also includes an integrated miniature preamplifier (30-dB amplification; ERA-8SM+, Mini-Circuits) on the ultrasound transducer to amplify the signal before transmission to the acquisition card, which improves the overall signal-to-noise ratio of the images. In addition, the use of cylindrical bundles that are raster-scanned together with the transducer instead of fixed rectangular bundles leads to more efficient illumination and better signal-to-noise ratio. The use of an articulated arm with three degrees of freedom (rotulas) and a single screw to simultaneously tighten (DG Holder, NOGA) all the rotulas improves the usability of the system.

The resolution of the system is ~30 μm (lateral) and ~7 μm (axial) up to ~1.2 mm deep. From 1.2 to 2.5 mm, the resolution worsens to 10 μm. Further degradation is expected beyond those depths due to the attenuation of the high-frequency components of the ultrasound signal by tissue. A detailed assessment on the resolution of the system can be found in (*9*).

Imaging identical sections of psoriasis plaques during conventional therapy

To image identical sections of the monitored psoriasis plaques in those patients undergoing conventional therapy, the area of interest was marked using two green ink dots (fig. S1). The dots were separated by a 4-mm gap, which corresponded to the width of the chosen transverse field of view. Before each imaging session, the scan head was first manually positioned using UB-RSOM 2G's detachable interface unit such that the ink dots macroscopically marked the limits of the field of view. Consequently, the ink dots' optoacoustic signals were identified using short preacquisitions. Then, the home position of the transducer was adjusted to maintain the field of view precisely between the dots, with them centered on the sagittal axis.

Quantification of disease hallmarks and correlation with PASI

Once images were acquired and reconstructed, the first step to obtain features resolved by UB-RSOM 2G was to flatten the skin surface in the reconstructed images. This step was performed manually as follows: The whole 3D image was divided into 20-μm-thick slices in the *y* direction (Fig. 1F). For each slice, the maximum intensity projection (MIP) along the *y* direction was calculated. In the MIPs, the skin surface can be observed univocally. For every MIP, the operator placed 10 points along the surface of the skin. Using an interpolation algorithm based on spline functions, whole surfaces were extracted and the skin was flattened (fig. S4). The MIP image along the *y* axis was subsequently computed from the flattened skin images.

The MCLL, MCLD, and MPW were calculated manually from the MIP (fig. S4). The total blood volume, fractal number of the vascular structures, and the ratio of low-to-high frequency content of the optoacoustic signal were calculated as explained in (*9*).

Statistical analysis

The repeatability coefficient was calculated as $1.96 \times \sqrt{2} \times$ std, where std is the within-subject SD and was calculated using an ANOVA using MATLAB, assuming normality in the error distribution. Normality was checked using the Anderson-Darling test. Data for the repeatability test are available in data file S1.

SUPPLEMENTARY MATERIALS

www.science.org/doi/10.1126/scitranslmed.abm8059
Materials and Methods
Figs. S1 to S5
Data file S1
MDAR Reproducibility Checklist

View/request a protocol for this paper from *Bio-protocol*.

REFERENCES AND NOTES

1. F. O. Nestle, D. H. Kaplan, J. Barker, Psoriasis. *N. Engl. J. Med.* **361**, 496–509 (2009).
2. W.-H. Boehncke, M. P. Schön, Psoriasis. *Lancet* **386**, 983–994 (2015).
3. T. Wong, L. Hsu, W. Liao, Phototherapy in psoriasis: A review of mechanisms of action. *J. Cutan. Med. Surg.* **17**, 6–12 (2013).
4. R. B. Warren, M. Gooderham, R. Burge, B. Zhu, D. Amato, K. H. Liu, D. Shrom, J. Guo, A. Brnabic, A. Blauvelt, Comparison of cumulative clinical benefits of biologics for the treatment of psoriasis over 16 weeks: Results from a network meta-analysis. *J. Am. Acad. Dermatol.* **82**, 1138–1149 (2020).

5. M. Augustin, K. Reich, PASImeter psoriasis severity index: Photographic guide; www.dermatools.net/dam/jcr:f95c96d7-cec5-4a25-ab3b-a1e3b2b4d5e0/PASIMETER-Photographic-Pr%C3%A4sentationmdus.pdf.
6. P. I. Spuls, L. L. A. Lecluse, M.-L. N. F. Poulsen, J. D. Bos, R. S. Stern, T. Nijsten, How good are clinical severity and outcome measures for psoriasis?: Quantitative evaluation in a systematic review. *J. Investig. Dermatol.* **130**, 933–943 (2010).
7. C. E. M. Griffiths, J. N. Barker, Pathogenesis and clinical features of psoriasis. *Lancet* **370**, 263–271 (2007).
8. C. Ryan, N. J. Korman, J. M. Gelfand, H. W. Lim, C. A. Elmets, S. R. Feldman, A. B. Gottlieb, J. Y. M. Koo, M. Lebwohl, C. L. Leonardi, A. S. van Voorhees, R. Bhushan, A. Menter, Research gaps in psoriasis: Opportunities for future studies. *J. Am. Acad. Dermatol.* **70**, 146–167 (2014).
9. J. Aguirre, M. Schwarz, N. Garzorz, M. Omar, A. Buehler, K. Eyerich, V. Ntziachristos, Precision assessment of label-free psoriasis biomarkers with ultra-broadband optoacoustic mesoscopy. *Nat. Biomed. Eng.* **1**, 0068 (2017).
10. B. Hindelang, J. Aguirre, M. Schwarz, A. Berezhnoi, K. Eyerich, V. Ntziachristos, T. Biedermann, U. Darsow, Non-invasive imaging in dermatology and the unique potential of raster-scan optoacoustic mesoscopy. *J. Eur. Acad. Dermatol. Venereol.* **33**, 1051–1061 (2019).
11. A. Berezhnoi, J. Aguirre, B. Hindelang, N. Garzorz-Stark, M. Omar, U. Darsow, K. Eyerich, V. Ntziachristos, Optical features of human skin revealed by optoacoustic mesoscopy in the visible and short-wave infrared regions. *Opt. Lett.* **44**, 4119–4122 (2019).
12. J. Aguirre, B. Hindelang, A. Berezhnoi, U. Darsow, F. Lauffer, K. Eyerich, T. Biedermann, V. Ntziachristos, Assessing nailfold microvascular structure with ultra-wideband raster-scan optoacoustic mesoscopy. *Photoacoustics* **10**, 31–37 (2018).
13. B. Hindelang, J. Aguirre, A. Berezhnoi, T. Biedermann, U. Darsow, B. Eberlein, V. Ntziachristos, Quantification of skin sensitivity to ultraviolet radiation using ultrawideband optoacoustic mesoscopy. *Br. J. Dermatol.* **184**, 352–354 (2021).
14. B. Hindelang, J. Aguirre, A. Berezhnoi, H. He, K. Eyerich, V. Ntziachristos, T. Biedermann, U. Darsow, Optoacoustic mesoscopy shows potential to increase accuracy of allergy patch testing. *Contact Dermatitis* **83**, 206–214 (2020).
15. F. Lacarrubba, G. Pellacani, S. Gurgone, A. E. Verzì, G. Micali, Advances in non-invasive techniques as aids to the diagnosis and monitoring of therapeutic response in plaque psoriasis: A review. *Int. J. Dermatol.* **54**, 626–634 (2015).
16. M. Agozzino, C. Noal, F. Lacarrubba, M. Ardigò, Monitoring treatment response in psoriasis: Current perspectives on the clinical utility of reflectance confocal microscopy. *Psoriasis (Auckl.)* **7**, 27–34 (2017).
17. M. Ardigò, M. Agozzino, C. Longo, A. Lallas, V. Di Lernia, A. Fabiano, A. Conti, I. Sperduti, G. Argenziano, E. Berardesca, G. Pellacani, Reflectance confocal microscopy for plaque psoriasis therapeutic follow-up during an anti-TNF-α monoclonal antibody: An observational multicenter study. *J. Eur. Acad. Dermatol. Venereol.* **29**, 2363–2368 (2015).
18. M. Omar, J. Aguirre, V. Ntziachristos, Optoacoustic mesoscopy for biomedicine. *Nat. Biomed. Eng.* **3**, 354–370 (2019).
19. S. C. A. Hanssen, C. J. M. van der Vleuten, P. E. J. van Erp, M. M. B. Seyger, P. C. M. van de Kerkhof, The effect of adalimumab on the vasculature in psoriatic skin lesions. *J. Dermatol. Treat.* **30**, 221–226 (2019).
20. I. M. Braverman, A. Yen, Ultrastructure of the human dermal microcirculation. II. The capillary loops of the dermal papillae. *J. Investig. Dermatol.* **68**, 44–52 (1977).
21. J. W. Bartlett, C. Frost, Reliability, repeatability and reproducibility: Analysis of measurement errors in continuous variables. *Ultrasound Obstet. Gynecol.* **31**, 466–475 (2008).
22. N. J. Schork, Personalized medicine: Time for one-person trials. *Nature* **520**, 609–611 (2015).
23. H. Morsy, S. Kamp, L. Thrane, N. Behrendt, B. Saunder, H. Zayan, E. A. Elmagid, G. B. E. Jemec, Optical coherence tomography imaging of psoriasis vulgaris: Correlation with histology and disease severity. *Arch. Dermatol. Res.* **302**, 105–111 (2010).
24. J. Welzel, M. Bruhns, H. H. Wolff, Optical coherence tomography in contact dermatitis and psoriasis. *Arch. Dermatol. Res.* **295**, 50–55 (2003).
25. K. Buder, P. Knuschke, G. Wozel, Evaluation of methylprednisolone aceponate, tacrolimus and combination thereof in the psoriasis plaque test using sum score, 20-MHz-ultrasonography and optical coherence tomography. *Int. J. Clin. Pharmacol. Ther.* **48**, 814–820 (2010).
26. J. Olsen, J. Holmes, G. B. Jemec, Advances in optical coherence tomography in dermatology—A review. *J. Biomed. Opt.* **23**, 1–10 (2018).
27. M. L. Musumeci, F. Lacarrubba, C. M. Fusto, G. Micali, Combined clinical, capillaroscopic and ultrasound evaluation during treatment of plaque psoriasis with oral cyclosporine. *Int. J. Immunopathol. Pharmacol.* **26**, 1027–1033 (2013).
28. F. Lacarrubba, B. Nardone, M. L. Musumeci, G. Micali, Ultrasound evaluation of clobetasol propionate 0.05% foam application in psoriatic and healthy skin: A pilot study. *Dermatol. Ther.* **22** Suppl 1, S19–S21 (2009).
29. G. Odorici, A. Losi, S. Ciardo, G. Pellacani, A. Conti, Non-invasive evaluation of Secukinumab efficacy in severe plaque psoriasis with confocal microscopy and optical coherence tomography: A case report. *Skin Res. Technol.* **24**, 160–162 (2018).
30. A. J. Deegan, F. Talebi-Liasi, S. Song, Y. Li, J. Xu, S. Men, M. M. Shinohara, M. E. Flowers, S. J. Lee, R. K. Wang, Optical coherence tomography angiography of normal skin and inflammatory dermatologic conditions. *Lasers Surg. Med.* **50**, 183–193 (2018).
31. S. Schuh, J. Holmes, M. Ulrich, L. Themstrup, G. B. E. Jemec, N. de Carvalho, G. Pellacani, J. Welzel, Imaging blood vessel morphology in skin: Dynamic optical coherence tomography as a novel potential diagnostic tool in dermatology. *Dermatol. Ther.* **7**, 187–202 (2017).
32. C. Errico, J. Pierre, S. Pezet, Y. Desailly, Z. Lenkei, O. Couture, M. Tanter, Ultrafast ultrasound localization microscopy for deep super-resolution vascular imaging. *Nature* **527**, 499–502 (2015).
33. C. Fink, C. Alt, L. Uhlmann, C. Klose, A. Enk, H. A. Haenssle, Precision and reproducibility of automated computer-guided Psoriasis Area and Severity Index measurements in comparison with trained physicians. *Br. J. Dermatol.* **180**, 390–396 (2019).
34. A. Stylogiannis, L. Prade, A. Buehler, J. Aguirre, G. Sergiadis, V. Ntziachristos, Continuous wave laser diodes enable fast optoacoustic imaging. *Photoacoustics* **9**, 31–38 (2018).
35. M. Xu, L. V. Wang, Universal back-projection algorithm for photoacoustic computed tomography. *Phys. Rev. E Stat. Nonlinear Soft Matter Phys.* **71**, 16706 (2005).
36. J. Aguirre, A. Berezhnoi, H. He, M. Schwarz, B. Hindelang, M. Omar, V. Ntziachristos, Motion quantification and automated correction in clinical RSOM. *IEEE Trans. Med. Imaging* **38**, 1340–1346 (2019).

Acknowledgments: We would like to thank R. J. Wilson for editing the manuscript. **Funding:** This project was funded by the German Society of Dermatology (DDG, German Psoriasis Price to J.A.), the European Commission ("INNODERM" no. 687866 and "WINTHER" no. 871763 to V.N.), and the German Research Foundation (DFG, 435874434/A2 to T.B.). **Author contributions:** Conceptualization: J.A., V.N., and B.H. Methodology: J.A. and B.H. Data curation: B.H., J.A., T.N., A.B., and L.E. Investigation: J.A. and B.H. Visualization: J.A. and A.B. Funding acquisition: J.A., V.N., and T.B. Project administration: J.A., V.N., U.D., and T.B. Supervision: J.A., V.N., U.D., T.B., K.E., and F.L. Writing—original draft: J.A., B.H., and V.N. **Competing interests:** J.A. is co-inventor of the patent applications EP2946721A1 and EP3654828A1 held by the Helmholtz Zentrum München that covers aspects of RSOM. V.N. has financial interests in iThera Medical GmbH. All other authors declare that they have no competing interests. **Data and materials availability:** All data associated with this study are present in the paper or the Supplementary Materials. Reasonable requests will be granted with permission of the Klinik und Poliklinik für Dermatologie und Allergologie am Biederstein, Munich, Germany. Figures in blue and green colormaps are available for the colorblind reader.

Submitted 13 October 2021
Accepted 19 April 2022
Published 11 May 2022
10.1126/scitranslmed.abm8059

Science Translational Medicine

Enabling precision monitoring of psoriasis treatment by optoacoustic mesoscopy

Benedikt Hindelang, Teresa Nau, Ludwig Englert, Andrei Berezhnoi, Felix Lauffer, Ulf Darsow, Tilo Biedermann, Kilian Eyerich, Juan Aguirre, and Vasilis Ntziachristos

Sci. Transl. Med., **14** (644), eabm8059.
DOI: 10.1126/scitranslmed.abm8059

More than skin-deep

Monitoring inflammatory skin diseases such as psoriasis is a subjective process that relies on clinical scores calculated from skin appearance. Here, Hindelang *et al.* developed ultra-broadband raster-scan optoacoustic mesoscopy (UB-RSOM), a type of noninvasive, label-free imaging that yields three-dimensional images of the skin including its microvasculature. Using the UB-RSOM system, the authors longitudinally monitored patients with psoriasis undergoing conventional treatment or biological treatment. They detected quantifiable changes in microvascular morphology in response to treatment, which were not detectable looking at surface skin and which correlated with dermatology life quality index. UB-RSOM could help monitor and optimize treatments for inflammatory skin conditions.

Science Translational Medicine (ISSN) is published by the American Association for the Advancement of Science. 1200 New York Avenue NW, Washington, DC 20005. The title *Science Translational Medicine* is a registered trademark of AAAS.